Auriel A. Willette,[1] Nina Modanlo,[2] and Dimitrios Kapogiannis,[1] for the Alzheimer's Disease Neuroimaging Initiative*

Insulin Resistance Predicts Medial Temporal Hypermetabolism in Mild Cognitive Impairment Conversion to Alzheimer Disease

Diabetes 2015;64:1933–1940 | DOI: 10.2337/db14-1507

Alzheimer disease (AD) is characterized by progressive hypometabolism on [^{18}F]-fluorodeoxyglucose positron emission tomography (FDG-PET) scans. Peripheral insulin resistance (IR) increases AD risk. No studies have examined associations between FDG metabolism and IR in mild cognitive impairment (MCI) and AD, as well as MCI conversion to AD. We studied 26 cognitively normal (CN), 194 MCI (39 MCI-progressors, 148 MCI-stable, 2 years after baseline), and 60 AD subjects with baseline FDG-PET from the Alzheimer's Disease Neuroimaging Initiative. Mean FDG metabolism was derived for AD-vulnerable regions of interest (ROIs), including lateral parietal and posteromedial cortices, medial temporal lobe (MTL), hippocampus, and ventral prefrontal cortices (vPFC), as well as postcentral gyrus and global cerebrum control regions. The homeostasis model assessment of IR (HOMA-IR) was used to measure IR. For AD, higher HOMA-IR predicted lower FDG in all ROIs. For MCI-progressors, higher HOMA-IR predicted higher FDG in the MTL and hippocampus. Control regions showed no associations. Higher HOMA-IR predicted hypermetabolism in MCI-progressors and hypometabolism in AD in medial temporal regions. Future longitudinal studies should examine the pathophysiologic significance of the shift from MTL hyper- to hypometabolism associated with IR.

Type 2 diabetes is a risk factor for Alzheimer disease (AD) (1,2). Peripheral insulin resistance (IR), broadly defined as reduced cellular response to insulin (3), also increases AD risk even without hyperglycemia (4). In certain brain regions with a high density of insulin receptors, insulin normally facilitates glucose metabolism (5). Interestingly, AD-related pathology and atrophy preferentially target these same temporal, prefrontal, and posteromedial parietal areas (6). In AD, these regions show disruption of insulin signaling (7), and the degree of disruption in at least the hippocampus is related to worse antemortem cognition (8). Furthermore, peripheral IR is associated with atrophy in these regions in aged rhesus macaques (9) and humans (10,11). The pathogenic significance of IR in AD is further highlighted by a recent study that showed brain IR preceding development of clinical AD (12).

Progressive brain hypometabolism is a hallmark of AD (13). Glucose metabolism is often assessed using [^{18}F]-fluorodeoxyglucose (FDG) positron emission tomography (PET). Lower FDG metabolism corresponds to declines in memory, executive function, and global cognition in mild cognitive impairment (MCI) and AD (14–16). There is preliminary evidence that IR inhibits glucose metabolism in AD-sensitive brain regions. For example, in euglycemic, healthy men with somatostatin-suppressed insulin secretion, insulin infusion stimulates regional metabolism in the prefrontal cortex (PFC), an effect that is diminished in men with IR (17). Among cognitively normal (CN), aged participants with hyperglycemia, higher peripheral IR corresponds to lower resting FDG metabolism in parietal, ventral PFC, and medial temporal lobe (MTL) areas, which

[1]Laboratory of Neurosciences, National Institute on Aging, Baltimore, MD
[2]Johns Hopkins University, Baltimore, MD

Corresponding author: Dimitrios Kapogiannis, kapogiannisd@mail.nih.gov.

Received 2 October 2014 and accepted 7 January 2015.

This article contains Supplementary Data online at http://diabetes.diabetesjournals.org/lookup/suppl/doi:10.2337/db14-1507/-/DC1.

A.A.W. is currently affiliated with the Department of Food Science and Human Nutrition, Iowa State University, Ames, IA

*A complete listing of Alzheimer's Disease Neuroimaging Initiative (ADNI) investigators can be found at http://adni.loni.usc.edu/wp-content/uploads/how_to_apply/ADNI_Acknowledgement_List.pdf.

are particularly vulnerable to AD pathology (18). In addition, intranasal insulin treatment in patients with MCI and early AD improves memory performance and maintains glucose metabolism in similar frontal, posteromedial, and temporal areas (14).

To date, no systematic study has been conducted of the association between peripheral IR and FDG metabolism in AD-vulnerable regions across the spectrum of CN older adults, patients with MCI who later progressed to AD or remained stable, or in those with early AD. To this end, we used Alzheimer's Disease Neuroimaging Initiative (ADNI) data to calculate the homeostatic model assessment of IR (HOMA-IR), an index of peripheral IR. We also derived FDG metabolism in AD-sensitive regions of interest (ROIs), including ventral PFC (vPFC), MTL, hippocampus, lateral parietal cortex, posteromedial cortex, as well as postcentral gyrus and global cerebrum control regions, and studied their associations with HOMA-IR. Finally, we investigated if HOMA-IR and FDG associations remained stable when enriching MCI and AD cohorts for amyloid-positivity.

RESEARCH DESIGN AND METHODS

Participants

Data used in the preparation of this article were obtained from the ADNI database (adni.loni.usc.edu). The ADNI was launched in 2003 by the National Institute on Aging, the National Institute of Biomedical Imaging and Bioengineering, the U.S. Food and Drug Administration, private pharmaceutical companies, and nonprofit organizations, as a $60 million, 5-year public-private partnership. The primary goal of ADNI has been to test whether serial MRI, PET, other biological markers, and clinical and neuropsychological assessment can be combined to measure the progression of MCI and early AD. The principal investigator of this initiative is Michael W. Weiner, MD, VA Medical Center and University of California-San Francisco.

The following baseline data were available for 26 CN, 194 MCI, and 60 AD participants:

1. demographic/anthropometric measures including age, sex, education, and BMI;
2. FDG-PET scans;
3. regional gray matter (GM) volumes;
4. fasting insulin and glucose;
5. apolipoprotein E (ApoE) ε4 genotype;
6. neuropsychological performance measures; and
7. clinical diagnosis at baseline and at month 24, as well as confirmation of MCI conversion by the ADNI Conversion Committee.

Data for cerebrospinal fluid or amyloid PET scans on 227 of 280 participants were also downloaded for a supplementary analysis (Supplementary Data). Participants were clinically diagnosed at the screening and each subsequent visit based on standardized criteria (19).

Participants with MCI at baseline who remained stable by 24 months were categorized as MCI-S (n = 148) versus participants who progressed to AD and were categorized as MCI-P (n = 39). To determine MCI conversion, MCI participants were seen at 0, 6, 12, 24, and 36 months and assessed for cognitive and general function. Briefly, for an MCI participant who met criteria for probable AD on a given visit, the site physician provided diagnostic data to the ADNI Conversion Committee, which reached a consensus regarding conversion. Probable AD was in part defined as *1*) a Clinical Dementia Rating of 0.5 or 1.0; *2*) abnormal, education-adjusted memory function on the Logical Memory II subscale; *3*) Mini-Mental State Examination (MMSE) inclusive of 20–26; and *4*) having met probable AD criteria defined by National Institute of Neurological and Communicative Diseases and Stroke/Alzheimer's Disease and Related Disorders Association. We refer readers to the ADNI1 procedural manual for further details (http://adni.loni.usc.edu/).

Standard Protocol Approvals, Registrations, and Patient Consents

Written informed consent was obtained from all ADNI participants at their respective ADNI sites. The ADNI protocol was approved by site-specific institutional review boards.

Insulin, Glucose, and HOMA-IR

As described in the ADNI1 protocol manual (http://adni.loni.usc.edu/), baseline blood samples were collected from subjects after overnight fasting. Insulin was assayed from plasma using a multiplex array (Human Discovery Map; Rules-Based Medicine, Austin, TX). The least detectable dose was 0.6 μU/mL. Glucose was assayed as part of routine blood work. HOMA-IR (20) and the quantitative insulin sensitivity check index (QUICKI) (21) were calculated from insulin and glucose values from the baseline visit. Baseline samples were collected within 14 days from baseline FDG-PET. Willette et al. (22) found that HOMA-IR is stable across at least 4 years in overweight, late middle-aged humans; therefore, our index of HOMA-IR very likely reflects IR at the time of the scan. Morris et al. (23) also used baseline glucose and insulin data in ADNI to compute QUICKI and determine glycemic groups for use in cognitive and imaging analyses. Participants were defined as hyperglycemic rather than euglycemic if their fasting blood glucose levels were 100 mg/dL or greater (American Diabetes Association criterion) or were taking medication or insulin to control type 2 diabetes.

Cognition and Clinical Stage Measures

Table 1 indicates values for the MMSE, AD assessment scale-cognitive subscale, the clinical dementia rating-sum of boxes, and previously derived ADNI factor scores for executive function (24) and memory (25).

MRI

Regional GM volumes were used to account for the potential effects of regional atrophy in FDG analyses, because expanding sulci in MCI and AD brains may lead to

Table 1—Sample demographic, cognitive, and metabolic indices

Index	CN *n* = 26	MCI* *n* = 194	AD *n* = 60	*P* value	MCI-S *n* = 148	MCI-P *n* = 39	*P* value
Age (years)	75.69 ± 5.68	75.17 ± 7.29	75.25 ± 7.26	0.943	75.26 ± 7.10	75.83 ± 7.22	0.671
Education (years)	15.34 ± 3.15	15.77 ± 2.90	14.80 ± 3.45	0.096	15.69 ± 2.96	15.92 ± 2.75	0.678
Sex				0.512			0.602
Female	15	132	38		102	25	
Male	11	62	22		46	14	
ApoE ε4 genotype				**<0.001**			**0.039**
$\varepsilon4^-$	23	91	17		73	12	
$\varepsilon4^+$	3	103	43		75	27	
CDR-sob	0.06 ± 0.16	1.53 ± 0.80	4.32 ± 1.54	**<0.001**	1.55 ± 0.82	1.61 ± 0.92	0.712
MMSE	28.73 ± 1.43	27.18 ± 1.69	23.90 ± 1.92	**<0.001**	27.26 ± 1.68	26.64 ± 1.57	**0.047**
ADAS-cog (11-item)	7.11 ± 3.01	10.75 ± 4.08	18.32 ± 6.12	**<0.001**	10.55 ± 3.81	12.94 ± 4.16	**0.001**
Memory factor	0.53 ± 0.53	0.02 ± 0.70	−1.00 ± 0.72	**<0.001**	0.04 ± 0.66	−0.32 ± 0.69	**0.004**
Executive function factor	0.77 ± 0.44	−0.03 ± 0.57	−0.85 ± 0.49	**<0.00l**	−0.02 ± 0.53	−0.33 ± 0.45	**0.001**
BMI (kg/m^2)	26.76 ± 3.48	26.30 ± 3.93	26.08 ± 3.83	0.761	26.33 ± 3.91	25.79 ± 3.56	0.454
Insulin (uU/mL)	2.98 ± 3.10	2.78 ± 3.08	2.41 ± 1.46	0.589	2.66 ± 2.68	3.34 ± 4.49	0.245
Glucose (mg/dL)	104.68 ± 30.17	101.18 ± 20.36	100.59 ± 20.88	0.718	100.44 ± 19.15	98.56 ± 18.11	0.593
QUICKI	0.45 ± 0.09	0.44 ± 0.06	0 45 ± 0.08	0.387	0.44 ± 0.06	0.44 ± 0.07	0.705
HOMA-IR	0.87 ± 1.10	0.71 ± 0.84	0.60 ± 0.40	0.270	−0.30 ± 0.31	−0.26 ± 0.37	0.538

Data are shown as *n* or as mean ± SD. Boldface values indicate statistical significance. ADAS-cog, Alzheimer Disease Assessment Scale–cognitive subscale; CDR-sob, Clinical Dementia Rating–sum of boxes. *The 194 MCI participants were classified as MCI-S (*n* = 148), MCI-P (*n* = 39), or CN (*n* = 7) according to the 24-month visit.

underestimation of FDG values (26). Mean regional GM corresponding to each ROI was downloaded from a hierarchical parcellation MRI data set made available in ADNI from Davatzikos and colleagues (27,28). This data set consisted of 264 volumetric regions derived from preprocessed T1 images using techniques previously described (27,28).

FDG-PET

FDG-PET acquisition and preprocessing details have been described elsewhere (29). Briefly, [^{18}F]-FDG (185 MBq) was injected intravenously. After approximately 30 min, six 5-min frames were acquired. Each frame of a given baseline image series was coregistered to the first acquired frame. The image series was aggregated into a dynamic image set. The image set was then averaged, reoriented to a standard 160 × 160 × 96 voxel spatial matrix of resliced 1.5 mm^3 voxels, intensity normalized, and smoothed with an 8-mm full width at half maximum kernel. We then normalized FDG-PET pixel intensity to the pons, due to its preserved glucose metabolism in AD (30), to derive the standardized uptake value ratio. This step removes interindividual variability in tracer metabolism. Images were spatially normalized to Montreal Neurological Institute space using an existing template in SPM8 (http://www.fil.ion.ucl.ac.uk/spm/software/spm8/).

Five bilateral ROIs (Supplementary Fig. 1) were defined using the Wake Forest PickAtlas (http://fmri.wfubmc.edu/software/PickAtlas). ROIs were selected based on previous studies examining progressive hypometabolism across the temporal progression of AD (31,32) or areas where glucose metabolism has been associated with IR (18). These ROIs included hippocampus, MTL, lateral parietal, posteromedial (precuneus and posterior cingulate cortex), and vPFC. Two control regions were also examined: *1*) global cerebrum, to assess the possibility of IR affecting glucose metabolism in a diffuse and regionally nonspecific manner; and *2*) postcentral gyrus, because it is not vulnerable to AD pathology and its glucose metabolism does not appear to be affected by IR (18).

ApoE ε4 Genotype

The ADNI Biomarker Core at the University of Pennsylvania conducted ApoE genotyping. We characterized participants as being "non-ApoE ε4" (i.e., zero ApoE ε4 alleles) or "ApoE ε4" (i.e., one to two ApoE ε4 alleles).

Statistical Analyses

All statistical analyses were conducted using SPSS 20.0 software (IBM Corp., Armonk, NY). All variables were normally distributed except for HOMA-IR, which was log-transformed to achieve normality. Linear mixed modeling, followed by least significant differences post hoc tests, was used to test whether demographics, cognition, and other variables differed by baseline diagnosis of CN, MCI, or AD (Table 1).

For each ROI, we performed separate linear mixed modeling for baseline diagnosis or MCI conversion (MCI-S, MCI-P). The dependent variable was the mean FDG-PET

standardized uptake value ratio for a given ROI. All models included the following covariates: age at baseline, sex, education, hyperglycemia status, ApoE ε4 genotype, and mean regional GM within the ROI examined. Exploratory analyses that also included BMI did not influence results (data not shown). We examined the main effect of baseline diagnosis or MCI conversion, anticipating a stepwise decrease in FDG-PET from CN to MCI to AD, and from MCI-S to MCI-P (33). We also examined the fixed effects of HOMA-IR and the interaction of HOMA-IR × baseline diagnosis or HOMA-IR × MCI conversion to assess whether HOMA-IR was differentially associated with glucose metabolism in CN versus MCI versus AD, or MCI-S versus MCI-P. Similar analyses were done with QUICKI and yielded nearly identical results (data not shown). We addressed type 1 error by using Holm-Bonferroni correction (34) for all analyses. This closed test procedure maintains a family-wise $\alpha = 0.05$ by requiring unadjusted P values of 0.05 divided by x, x being the number of null hypotheses tested. For example, when testing five ROIs, a P value of 0.010 is needed among one of the tested ROIs for the test to achieve significance, followed by 0.013, 0.017, 0.025, and 0.050. For significant interactions, we performed follow-up analyses for each baseline diagnosis or MCI conversion group (35) to assess whether a significant linear association existed between HOMA-IR and FDG metabolism in one or more groups.

RESULTS

Demographics, Cognition, and IR Biomarkers

Diagnostic groups did not differ by age, sex, or education (Table 1). As expected, cognitive scores were lower and the proportion of non-ApoE ε4 versus ApoE ε4 increased from CN to MCI to AD participants as well as from MCI-S to MCI-P in a step-wise manner (data not shown). No significant differences were found for insulin, glucose, BMI, HOMA-IR, or QUICKI.

ROI Analysis: Differences in FDG Metabolism by Clinical Diagnosis and MCI Conversion

For each of the five ROIs and two control regions, separate mixed models were used to test effects of baseline diagnosis (CN, MCI, AD) or MCI conversion (MCI-S, MCI-P). Supplementary Table 1 reports lower FDG metabolism in a stepwise manner from CN to MCI to AD for global cerebrum, lateral parietal, posteromedial parietal, and hippocampus ROIs. Ventral PFC and MTL showed lower FDG metabolism for MCI versus CN and AD versus CN, but not AD versus MCI. No differences in FDG-PET metabolism were found for MCI-P versus MCI-S. No differences were noted for postcentral gyrus. Supplementary Fig. 2 illustrates the step-wise differences for MTL as an example. These results suggest that this ADNI subcohort shows the typical progressive hypometabolism from CN, to MCI, to AD (31–33).

ROI Analysis: HOMA-IR and FDG Metabolism Associations

The following analyses were conducted in the cohort (n = 280). Supplementary Text 1 describes a supplemental analysis among 227 participants, where MCI and AD groups were enriched for amyloid-positive status. All results for the amyloid-positive analysis are similar to findings described below.

MTL and Hippocampus

For hippocampus but not MTL, the HOMA-IR main effect surpassed Holm-Bonferroni correction (Supplementary Table 1). Significant HOMA-IR × baseline diagnosis interactions were seen for both hippocampus and MTL (Table 2). Figure 1 illustrates that higher HOMA-IR corresponded to less MTL FDG metabolism for AD, whereas no significant relationships were seen for CN or MCI. Among MCI participants, the main effect of HOMA-IR was nonsignificant (Supplementary Table 1), but there was a significant HOMA-IR × MCI conversion interaction (Table 2). Follow-up analyses indicated that higher HOMA-IR predicted more FDG metabolism in MCI-P and had no significant association with MCI-S (Fig. 2 depicts MTL results). Therefore, higher HOMA-IR predicted less FDG metabolism in the MTL and hippocampus among AD participants but higher FDG for MCI participants who progressed to AD by 24 months.

vPFC

Among all participants, the main effect of HOMA-IR was not significant (Supplementary Table 1), but there was a significant HOMA-IR × baseline diagnosis interaction (Table 2). As shown in Supplementary Fig. 3, higher IR predicted less PFC FDG metabolism only in AD patients, whereas no significant associations were seen for CN or MCI. Among MCI participants, the main effect of HOMA-IR was nonsignificant (Supplementary Table 1), but there was a significant HOMA-IR × MCI conversion interaction (Table 2). Follow-up analyses indicated that higher HOMA-IR was associated with lower FDG metabolism for MCI-S but had no significant association for MCI-P (Supplementary Fig. 4). Importantly, this pattern differed from temporal regions, where higher HOMA-IR predicted hypermetabolism for MCI-P and had no significant relationship for MCI-S. Among AD participants, by contrast, higher HOMA-IR predicted lower FDG metabolism in the prefrontal and temporal areas.

Lateral Parietal and Posteromedial Cortices

Results were similar for lateral parietal and posteromedial ROIs. Among all participants, the main effects of HOMA-IR were nonsignificant (Supplementary Table 1), but the HOMA-IR × baseline diagnosis interactions were significant (Table 2). Higher IR again predicted lower FDG metabolism in the lateral and posteromedial parietal regions for AD, whereas associations for CN or MCI were nonsignificant. Among MCI participants, the main effects of HOMA-IR (Supplementary Table 1) and the

Figure 1—Associations between HOMA-IR and MTL FDG metabolism among baseline diagnosis groups. The "blue circle," "green triangle," and "red star" symbols correspond, respectively, to CN, MCI, and AD participants. The R^2 value refers to the proportion of variance in FDG metabolism explained by HOMA-IR for a given group. Covariates included age at baseline, sex, education, hyperglycemia status, ApoE ε4 genotype, and mean MTL GM volume. SUVR, standardized uptake value ratio. *$P \leq 0.05$.

HOMA-IR × MCI conversion interactions (Table 2) were nonsignificant.

Control Regions: Global Cerebrum and Postcentral Gyrus

No significant main effects or interactions were noted for HOMA-IR or HOMA-IR × baseline diagnosis for either control area (Table 2 and Supplementary Table 1). Among MCI

Figure 2—Associations between HOMA-IR and MTL FDG metabolism by MCI conversion. The "green star" and "red square" symbols correspond to MCI participants who remained stable (MCI-S) or progressed to AD (MCI-P) by 24 months after baseline. The R^2 value refers to the proportion of variance in FDG metabolism explained by HOMA-IR for a given group. Covariates included age at baseline, sex, education, hyperglycemia status, ApoE ε4 genotype, and mean MTL GM volume. Importantly, the HOMA-IR and FDG-PET association for MCI-P remained similar after removing one log HOMA-IR value (0.87) three SDs from the group mean (R^2 = 0.307, P = 0.008), or that value and another case that was two SDs from the group mean (R^2 = 0.148, P = 0.048). SUVR, standardized uptake value ratio. ***$P \leq 0.001$.

Table 2—Interaction effects and HOMA-IR on ROI FDG metabolism

Region	Baseline diagnosis		MCI conversion		Model estimates for HOMA-IR ± SE				
	F value	*P* value	*F* value	*P* value	CN	MCI	AD	MCI-S	MCI-P
Postcentral gyrus	2.545	0.112[a]	0.308	0.580[a]	0.202 ± 0.365	−0.138 ± 0.076	−0.298 ± 0.178	−0.144 ± 0.096	−0.082 ± 0.215
Global cerebrum	2.572	0.110[a]	2.984	0.086[a]	−0.018 ± 0.011	0.003 ± 0.003	−0.003 ± 0.006	−0.030 ± 0.028	0.031 ± 0.053
Lateral parietal	6.351	**0.012**[b]	0.795	0.374[b]	0.148 ± 0.083	−0.027 ± 0.031	**−0.099 ± 0.050***	−0.037 ± 0.037	−0.005 ± 0.083
Precuneus + PCC	6.846	**0.009**[b]	0.660	0.418[b]	0.094 ± 0.129	−0.030 ± 0.035	**−0.161 ± 0.073***	−0.033 ± 0.043	0.004 ± 0.083
Hippocampus	5.857	**0.016**[b]	6.419	**0.012**[b]	0.073 ± 0.044	0.035 ± 0.018	**−0.076 ± 0.032***	0.008 ± 0.023	**0.098 ± 0.029****
MTL	4.834	**0.029**[b]	8.087	**0.005**[b]	0.052 ± 0.044	0.029 ± 0.017	**−0.074 ± 0.034***	−0.004 ± 0.018	**0.099 ± 0.020*****
VPFC	5.052	**0.025**[b]	5.856	**0.017**[b]	0.135 ± 0.065	−0.013 ± 0.025	**−0.172 ± 0.048*****	**−0.051 ± 0.029***	0.074 ± 0.047

Fixed-effect *F* statistics with corresponding levels of significance, followed by model parameter estimates and SE, from the mixed models for the ROIs. PCC, posterior cingulate cortex. [a]Both control regions (postcentral gyrus, global cerebrum FDG metabolism) were tested separately from ROIs. Holm-Bonferroni type 1 error correction required successive *P* values of 0.025 and 0.050 for interactions to be considered significant. [b]For each set of 5 ROIs per diagnostic group, Holm-Bonferroni type 1 error correction required successive *P* values of 0.010, 0.013, 0.017, 0.025, and 0.050 for interactions to be considered significant. Boldface text indicates significant *P* values. The model parameter estimate ± SE is for a given diagnostic group. *$P \leq 0.05$. **$P \leq 0.01$. ***$P \leq 0.001$.

participants, the HOMA-IR main effects and HOMA-IR × MCI conversion interactions were also nonsignificant.

DISCUSSION

In this study, we examined the relationships among peripheral IR, baseline diagnosis or MCI conversion, and mean FDG metabolism within several ROIs targeted by AD and two control regions.

Our ADNI subsample was typical in showing progressive hypometabolism from CN to MCI to AD (31–33). Clinical groups did not show differences in HOMA-IR. However, significant interactions were found between the baseline diagnosis and HOMA-IR in all ROIs as well as interactions between MCI conversion and HOMA-IR for temporal and frontal areas. These results suggest that IR may be differentially associated with FDG metabolism depending on disease status. No HOMA-IR associations were found for the global cerebrum or postcentral gyrus control regions. Higher HOMA-IR predicted less FDG metabolism in all temporal, parietal, and frontal areas for AD participants, whereas associations were nonsignificant for CN or MCI participants. Baker et al. (18) similarly found that higher HOMA-IR predicts less FDG metabolism in these areas in hyperglycemic, CN elderly individuals. Intranasal insulin therapy maintains FDG metabolism over time in these regions in MCI and early AD patients (14). The association of IR with glucose metabolism in these ROIs is further validated by findings that postprandial hyperglycemia (36) or somatostatin-suppressed subphysiologic insulin infusion (17) also modulate FDG metabolism in these regions.

Three findings were of particular interest: First, in MCI-P participants, higher HOMA-IR predicted hypermetabolism in the hippocampus and MTL. Second, in MCI-S participants, higher HOMA-IR predicted vPFC hypometabolism. Third, in AD participants, higher HOMA-IR was associated with hypometabolism in hippocampus and MTL as well as the other ROIs. Collectively, these findings suggest that during the MCI stage, HOMA-IR is differentially associated with either hypo- or hypermetabolism in different brain areas, depending on whether participants progress to develop clinical AD. We depict these differential associations in Fig. 3. Regionally specific patterns of hypo- and hypermetabolism or hypo- and hyperactivation (with FDG-PET and functional MRI, respectively) have been seen in populations at risk for AD and have been implicated in the transition to clinical AD. Hyperactivation and increased functional connectivity of the hippocampus and MTL has been proposed as an early compensatory response to the presence of amyloid in default mode network regions (37–39). Middle-aged, predemented individuals with Down syndrome, who are at high risk for AD, also show relative MTL hypermetabolism (40), as do aged individuals with subjective memory impairment (41). In addition, higher mean amyloid deposition in the precuneus corresponds to hypermetabolism in MCI and hypometabolism in AD in frontal and parietoccipital areas

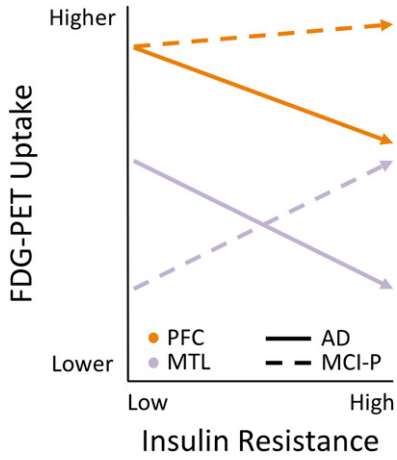

Figure 3—Differential associations of HOMA-IR and regional FDG uptake in MCI-P and AD. A hypothetical schematic shows how the association between HOMA-IR and FDG metabolism varies as a function of clinical diagnosis. For AD participants (solid line), higher HOMA-IR predict lower FDG in PFC ("orange" color) and MTL ("purple" color) regions. For the MCI-P participants (dashed lines), the HOMA-IR association with PFC FDG uptake is flat or may be slightly, albeit nonsignificantly, positive. By contrast, the HOMA-IR and MTL FDG association is clearly positive.

(42), suggesting that this hyperactivation is transient and gives way to hypoactivation in AD.

Previous studies have also shown positive associations between measures related to IR and brain indices, such as volume, in MCI/early AD and aged monkeys. Higher insulin area under the curve from a glucose tolerance test, which reflects higher IR, predicts better cognitive performance and more hippocampal volume cross-sectionally (43) and longitudinally (44) in MCI/early AD. Similarly, in aged rhesus macaques not on long-term calorie restriction, less insulin sensitivity is related to higher hippocampal volume (9). The underlying mechanism behind these IR associations with volume and FDG metabolism in the MTL in MCI/early AD is currently unclear. Hyperinsulinemia, a feature of IR, is related to higher insulin concentrations in the brain (45). Higher brain insulin concentrations may reduce amyloid oligomerization and toxicity (46), increase synaptogenesis (47), or modulate long-term potentiation and depression in the hippocampus to improve learning and memory (45). These phenomena may be the basis of a compensatory effect of IR at some transient stage during AD pathogenesis. Also unclear is whether IR directly affects FDG through changes in glucose metabolism or indirectly. Talbot et al. (8) found that physiologic and supraphysiologic insulin administration in CN and AD postmortem hippocampal tissue did not affect glucose metabolism. Yet, insulin infusion in somatostatin-suppressed men (17) or intranasal insulin in MCI and AD both affected MTL FDG metabolism (14). Alternatively, a potential indirect mechanism underlying IR and FDG associations may be differences in regional amyloid deposition. Higher amyloid in the precuneus, as

measured by Pittsburgh Compound B, corresponds to hypermetabolism in MCI and hypometabolism in AD (42).

As a limitation, our sample size for CN was small, and thus, the lack of associations for this group should be interpreted with caution. Our most intriguing finding was the positive relationship of HOMA-IR with MTL and hippocampus FDG in MCI-P, in line with the findings of higher resting state activity or FDG metabolism in MTL (37–42) as well as higher IR and higher hippocampal volume in MCI/early AD participants and aged rhesus monkeys (9,43,44). Our findings further motivate ongoing therapeutic efforts for treating AD by targeting peripheral and/or central IR, including the on-going clinical trials of exenatide (NCT01255163) and intranasal insulin (NCT01767909), and support their rationale of recruiting subjects at the stage of MCI when IR may be exercising different effects from those seen in AD. Completion of these and future trials will ultimately test whether targeting IR is a viable strategy for AD therapeutics.

Acknowledgments. The authors thank Drs. Eleanor Simonsick and Chee Chia, of the National Institute on Aging, for reviewing the manuscript before submission.

Funding. This research was supported in part by the Intramural Research Program of the National Institutes of Health, National Institute on Aging. Data collection and sharing for this project were funded by the ADNI (National Institutes of Health Grant U01-AG-024904) and Department of Defense ADNI (award number W81XWH-12-2-0012). ADNI is funded by the National Institute on Aging, the National Institute of Biomedical Imaging and Bioengineering, and through generous contributions from the Alzheimer's Association and the Alzheimer's Drug Discovery Foundation. The Canadian Institutes of Health Research is providing funds to support ADNI clinical sites in Canada. Private-sector contributions are facilitated by the Foundation for the National Institutes of Health (www.fnih.org). The grantee organization is the Northern California Institute for Research and Education, and the study is coordinated by the Alzheimer's Disease Cooperative Study at the University of California, San Diego. ADNI data are disseminated by the Laboratory for Neuro Imaging at the University of Southern California.

The data used in the preparation of this article were obtained from the ADNI database (adni.loni.usc.edu). As such, the investigators within the ADNI contributed to the design and implementation of ADNI and/or provided data but did not participate in analysis or writing of this report.

Duality of Interest. ADNI is funded by BioClinica, Inc., Biogen Idec, Inc., Bristol-Myers Squibb Company, Eisai Co., Ltd., Élan Pharmaceuticals, Inc., Eli Lilly and Company, F. Hoffmann-La Roche Ltd. and its affiliated company Genentech, Inc., GE Healthcare, Innogenetics, NV, IXICO Ltd., Janssen Alzheimer Immunotherapy Research & Development, LLC, Johnson & Johnson Pharmaceutical Research & Development LLC, Medpace, Inc., Merck & Co., Inc., Meso Scale Diagnostics, LLC, NeuroRx Research, Novartis Pharmaceuticals Corporation, Pfizer, Inc., Piramal Imaging, Servier, Synarc, Inc., and Takeda Pharmaceutical Company. No other potential conflicts of interest relevant to this article were reported.

Author Contributions. A.A.W. conceptualized and designed the study, analyzed and interpreted the data, and wrote and revised the manuscript for intellectual content. N.M. collected and interpreted the data and revised the manuscript for intellectual content. D.K. conceptualized and designed the study, analyzed and interpreted the data, and revised the manuscript for intellectual content. D.K. is the guarantor of this work and, as such, had full access to all the data in the study and takes responsibility for the integrity of the data and the accuracy of the data analysis.

References

1. Irie F, Fitzpatrick AL, Lopez OL, et al. Enhanced risk for Alzheimer disease in persons with type 2 diabetes and APOE epsilon4: the Cardiovascular Health Study Cognition Study. Arch Neurol 2008;65:89–93

2. Yaffe K, Falvey C, Hamilton N, et al. Diabetes, glucose control, and 9-year cognitive decline among older adults without dementia. Arch Neurol 2012;69:1170–1175

3. Goldstein BJ. Insulin resistance as the core defect in type 2 diabetes mellitus. Am J Cardiol 2002;90:3G–10G

4. Schrijvers EM, Witteman JC, Sijbrands EJ, Hofman A, Koudstaal PJ, Breteler MM. Insulin metabolism and the risk of Alzheimer disease: the Rotterdam Study. Neurology 2010;75:1982–1987

5. Cersosimo E, DeFronzo RA. Insulin resistance and endothelial dysfunction: the road map to cardiovascular diseases. Diabetes Metab Res Rev 2006;22:423–436

6. Craft S. The role of metabolic disorders in Alzheimer disease and vascular dementia: two roads converged. Arch Neurol 2009;66:300–305

7. Craft S, Watson GS. Insulin and neurodegenerative disease: shared and specific mechanisms. Lancet Neurol 2004;3:169–178

8. Talbot K, Wang HY, Kazi H, et al. Demonstrated brain insulin resistance in Alzheimer's disease patients is associated with IGF-1 resistance, IRS-1 dysregulation, and cognitive decline. J Clin Invest 2012;122:1316–1338

9. Willette AA, Bendlin BB, Colman RJ, et al. Calorie restriction reduces the influence of glucoregulatory dysfunction on regional brain volume in aged rhesus monkeys. Diabetes 2012;61:1036–1042

10. Rasgon NL, Kenna HA, Wroolie TE, et al. Insulin resistance and hippocampal volume in women at risk for Alzheimer's disease. Neurobiol Aging 2011;32:1942–1948

11. García-Casares N, Berthier ML, Jorge RE, et al. Structural and functional brain changes in middle-aged type 2 diabetic patients: a cross-sectional study. J Alzheimers Dis 2014;40:375–386

12. Kapogiannis D, Boxer A, Schwartz JB, et al. Dysfunctionally phosphorylated IRS-1 in neural-derived blood exosomes of preclinical Alzheimer's disease. FASEB J. 23 October 2014 [Epub ahead of print]

13. Mosconi L, Brys M, Glodzik-Sobanska L, De Santi S, Rusinek H, de Leon MJ. Early detection of Alzheimer's disease using neuroimaging. Exp Gerontol 2007;42:129–138

14. Craft S, Baker LD, Montine TJ, et al. Intranasal insulin therapy for Alzheimer disease and amnestic mild cognitive impairment: a pilot clinical trial. Arch Neurol 2012;69:29–38

15. Chen K, Ayutyanont N, Langbaum JB, et al.; Alzheimer's Disease Neuroimaging Initiative. Characterizing Alzheimer's disease using a hypometabolic convergence index. Neuroimage 2011;56:52–60

16. Shokouhi S, Claassen D, Kang H, et al. Longitudinal progression of cognitive decline correlates with changes in the spatial pattern of brain 18F-FDG PET. J Nucl Med 2013;54:1564–1569

17. Anthony K, Reed LJ, Dunn JT, et al. Attenuation of insulin-evoked responses in brain networks controlling appetite and reward in insulin resistance: the cerebral basis for impaired control of food intake in metabolic syndrome? Diabetes 2006;55:2986–2992

18. Baker LD, Cross DJ, Minoshima S, Belongia D, Watson GS, Craft S. Insulin resistance and Alzheimer-like reductions in regional cerebral glucose metabolism for cognitively normal adults with prediabetes or early type 2 diabetes. Arch Neurol 2011;68:51–57

19. Petersen RC. Mild cognitive impairment as a diagnostic entity. J Intern Med 2004;256:183–194

20. Matthews DR, Hosker JP, Rudenski AS, Naylor BA, Treacher DF, Turner RC. Homeostasis model assessment: insulin resistance and beta-cell function from fasting plasma glucose and insulin concentrations in man. Diabetologia 1985;28:412–419

21. Katz A, Nambi SS, Mather K, et al. Quantitative insulin sensitivity check index: a simple, accurate method for assessing insulin sensitivity in humans. J Clin Endocrinol Metab 2000;85:2402–2410

22. Willette AA, Xu G, Johnson SC, et al. Insulin resistance, brain atrophy, and cognitive performance in late middle-aged adults. Diabetes Care 2013;36:443–449
23. Morris JK, Vidoni ED, Honea RA, Burns JM; Alzheimer's Disease Neuroimaging Initiative. Impaired glycemia increases disease progression in mild cognitive impairment. Neurobiol Aging 2014;35:585–589
24. Gibbons LE, Carle AC, Mackin RS, et al.; Alzheimer's Disease Neuroimaging Initiative. A composite score for executive functioning, validated in Alzheimer's Disease Neuroimaging Initiative (ADNI) participants with baseline mild cognitive impairment. Brain Imaging Behav 2012;6:517–527
25. Crane PK, Carle A, Gibbons LE, et al.; Alzheimer's Disease Neuroimaging Initiative. Development and assessment of a composite score for memory in the Alzheimer's Disease Neuroimaging Initiative (ADNI). Brain Imaging Behav 2012;6:502–516
26. Samuraki M, Matsunari I, Chen WP, et al. Partial volume effect-corrected FDG PET and grey matter volume loss in patients with mild Alzheimer's disease. Eur J Nucl Med Mol Imaging 2007;34:1658–1669
27. Ou Y, Sotiras A, Paragios N, Davatzikos C. DRAMMS: deformable registration via attribute matching and mutual-saliency weighting. Med Image Anal 2011;15:622–639
28. Ou Y, Akbari H, Bilello M, Da X, Davatzikos C. Comparative evaluation of registration algorithms in different brain databases with varying difficulty: results and insights. IEEE Trans Med Imaging 2014;33:2039–2065
29. Jagust WJ, Bandy D, Chen K, et al. The Alzheimer's Disease Neuroimaging Initiative positron emission tomography core. Alzheimers Dement 2010;6:221–229
30. Minoshima S, Frey KA, Foster NL, Kuhl DE. Preserved pontine glucose metabolism in Alzheimer disease: a reference region for functional brain image (PET) analysis. J Comput Assist Tomogr 1995;19:541–547
31. Dukart J, Mueller K, Villringer A, et al.; Alzheimer's Disease Neuroimaging Initiative. Relationship between imaging biomarkers, age, progression and symptom severity in Alzheimer's disease. Neuroimage Clin 2013;3:84–94
32. Ewers M, Brendel M, Rizk-Jackson A, et al.; Alzheimer's Disease Neuroimaging Initiative (ADNI). Reduced FDG-PET brain metabolism and executive function predict clinical progression in elderly healthy subjects. Neuroimage Clin 2014;4:45–52
33. Weiner MW, Veitch DP, Aisen PS, et al. The Alzheimer's Disease Neuroimaging Initiative: a review of papers published since its inception. Alzheimers Dement 2012;8:S1–S68
34. Holm S. A simple sequentially rejective multiple test procedure. Scand J Stat 1979;6:65–70
35. Aiken L, West S. *Multiple Regression: Testing and Interpreting Interactions*. Newbury Park, CA, Sage, 1991
36. Kawasaki K, Ishii K, Saito Y, Oda K, Kimura Y, Ishiwata K. Influence of mild hyperglycemia on cerebral FDG distribution patterns calculated by statistical parametric mapping. Ann Nucl Med 2008;22:191–200
37. Mormino EC, Smiljic A, Hayenga AO, et al. Relationships between β-amyloid and functional connectivity in different components of the default mode network in aging. Cereb Cortex 2011;21:2399–2407
38. Miller SL, Celone K, DePeau K, et al. Age-related memory impairment associated with loss of parietal deactivation but preserved hippocampal activation. Proc Natl Acad Sci U S A 2008;105:2181–2186
39. Sperling RA, Dickerson BC, Pihlajamaki M, et al. Functional alterations in memory networks in early Alzheimer's disease. Neuromolecular Med 2010;12:27–43
40. Haier RJ, Alkire MT, White NS, et al. Temporal cortex hypermetabolism in Down syndrome prior to the onset of dementia. Neurology 2003;61:1673–1679
41. Scheef L, Spottke A, Daerr M, et al. Glucose metabolism, gray matter structure, and memory decline in subjective memory impairment. Neurology 2012;79:1332–1339
42. Cohen AD, Price JC, Weissfeld LA, et al. Basal cerebral metabolism may modulate the cognitive effects of Abeta in mild cognitive impairment: an example of brain reserve. J Neurosci 2009;29:14470–144778
43. Burns JM, Donnelly JE, Anderson HS, et al. Peripheral insulin and brain structure in early Alzheimer disease. Neurology 2007;69:1094–1104
44. Burns JM, Honea RA, Vidoni ED, Hutfles LJ, Brooks WM, Swerdlow RH. Insulin is differentially related to cognitive decline and atrophy in Alzheimer's disease and aging. Biochim Biophys Acta 2012;1822:333–339
45. Kleinridders A, Ferris HA, Cai W, Kahn CR. Insulin action in brain regulates systemic metabolism and brain function. Diabetes 2014;63:2232–2243
46. De Felice FG, Vieira MN, Bomfim TR, et al. Protection of synapses against Alzheimer's-linked toxins: insulin signaling prevents the pathogenic binding of Abeta oligomers. Proc Natl Acad Sci U S A 2009;106:1971–1976
47. Chiu SL, Chen CM, Cline HT. Insulin receptor signaling regulates synapse number, dendritic plasticity, and circuit function in vivo. Neuron 2008;58:708–719